Supplement of Atmos. Chem. Phys., 18, 7237–7250, 2018
https://doi.org/10.5194/acp-18-7237-2018-supplement

Atmospheric Chemistry and Physics
Open Access

Supplement of

Competition for water vapour results in suppression of ice formation in mixed-phase clouds

Emma L. Simpson et al.

Correspondence to: Gordon McFiggans (g.mcfiggans@manchester.ac.uk)

1 Sensitivities to model bin structure

Three bin structures are compared in Supplementary Fig. S1., which reveals sensitivities to the bin structure used. The full moving structure allows particles in each size bin grow to their exact size. Particles are not moved between size bins. Instead the size of the bin changes as particles grow (or shrink). This structure does not allow processes such as collision coalescence or particle nucleation as the appropriate size bin for new particles may not exist as bin sizes continually change. However the full moving structure provides the most accurate representation of microphysical processes as particles retain their exact size. The other two bin structures in Supplementary Fig. S1., move particles between fixed size bins, and therefore do not allow particles to retain the exact sizes they grow (or shrink) to. In the quasistationary and moving centre bin structures particles grow to their exact size in one time step and are then fitted back onto grid of fixed bin sizes. The method in which particles are fitted back onto a grid varies between the two structures (see Jacobson (1999) for more details). Using a fixed grid allows collision coalescence and particle nucleation to be represented as the appropriate size bin for new particles always exists. However particles do not retain their exact size and are instead put into a size bin closest to their exact size or their volume is averaged between two adjacent bins. This can result in irregularities and numerical diffusion in results. For this reason and the fact that we do not consider particle nucleation or collision coalescence in our study we use the full moving structure in order to provide the best representation of particles in our simulations.

Supplementary Fig. S1., reveals a non-monotonic relationship between INP diameter and frozen fraction. Focusing on the 'full moving ice' line (solid black line), the frozen fraction initially increases with particle diameter. This is because the concentration of ice active sites increases with surface area, i.e. the potential for a particle to nucleate ice increases. At the same time the fraction of activated drops decreases with increasing particle size. This is because larger particles are not able to activate due to kinetic limitations to growth. As particle size increases between approx. 800 nm to 1000 nm the number of ice crystals decreases. Here the ability of a particle to nucleate ice is not limited by the number of active sites presents as the particles have a sufficiently large surface area, but are limited by the mass of water condensed onto their surface. These particles are not able to achieve the threshold mass of water required for freezing to proceed. As particle size increases beyond 1000 nm, the fraction of frozen particle increases. Here particles are sufficiently large to be able to achieve the threshold mass of water required for freezing, and thus the frozen fraction increases with particle diameter. At larger particle sizes the mass of water required for freezing is less than that required to activate into a cloud drop, therefore the fraction of activated drops decreases with particle diameter.

2 Idealised suppression case

Supplementary Fig. S2. shows an idealised case demonstrating the suppression of ice formation caused by the presence of CCN when the criteria for heterogeneous freezing is *Activated only*.

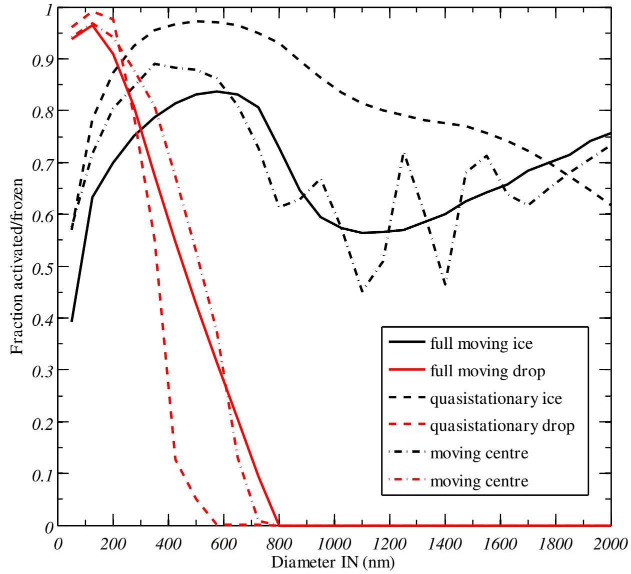

Figure S1. Comparison of the three bin structures available in ACPIM, full moving, quasistationary and moving center. For more details on these bin structures refer to Jacobson (1999). One mode of INP with a concentration of 10 cm^{-3} was used here.

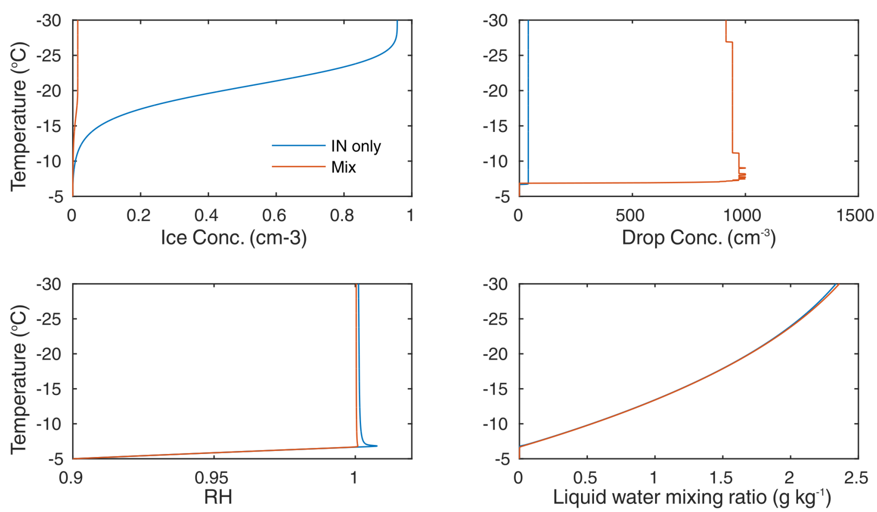

Figure S2. The *low CCN* case (blue lines) contained 1 L^{-1} 300 nm K-feldspar and 50 cm^{-3} 60 nm ammonium sulphate particles. The *high CCN* case (red lines) contained 1 L^{-1} 300 nm K-feldspar and 2000 cm^{-3} 200 nm ammonium sulphate particles. Initial conditions for the two simulations are the same as those detailed in Table 3. An updraft velocity of 0.5 ms^{-1} was used in both cases. The criteria for heterogeneous freezing was that only activated INPs could freeze. Top left panel shows the number concentration of ice with decreasing temperature. Top right panel shows the droplet number concentration with decreasing temperature. Bottom left panel shows the relative humidity with respect to water with decreasing temperature. Bottom right panel shows the liquid water mixing ratio with decreasing temperature.

3 Example lognormal fits for aerosol in chamber experiments

Supplementary Figures S3 and S4 give examples of the lognormal fits used to represent the aerosol present in the chamber in model simulations.

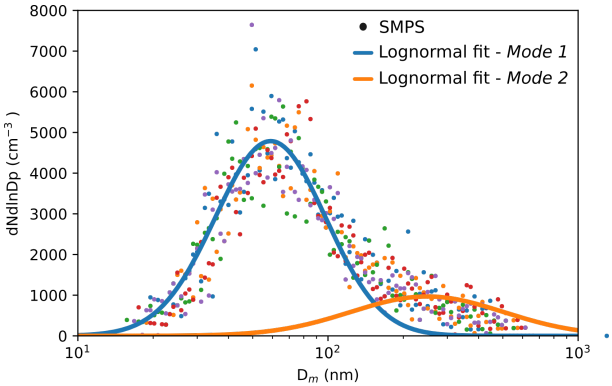

Figure S3. Example lognormal fit for ammonium sulphate particles. Coloured circles are measurements made by the SMPS instrument while the blue and orange lines are the lognormal fits used as initial conditions in ACPIM.

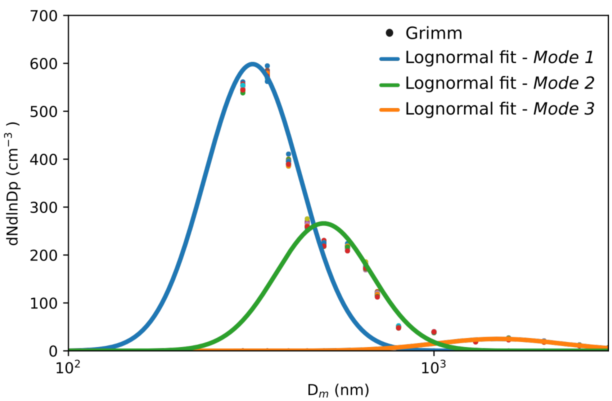

Figure S4. Example lognormal fit for K-feldspar particles. Coloured circles are measurements made by the GRIMM instrument while the blue, green and orange lines are the lognormal fits used as initial conditions in ACPIM.

The values for all lognormal fits used in model simulations shown in Supplementary Fig. S6 are given in Supplementary Table 1. In experiments shown in Supplementary Fig. S6 panels d and f two lognormal modes were required to represent the ammonium sulphate size distribution, as shown in Supplementary Fig. S3. In all other experiments that contain ammonium sulphate one lognormal mode was sufficient to represent the aerosol size distribution.

	K-feldspar			Ammonium Sulphate		
Fig. Panel	N (cm^{-3})	D (μm)	ln σ	N (cm^{-3})	D (μm)	ln σ
a	[400,200,7]	[0.32,0.5,1.5]	[0.3,0.3,0.4]	0	0	0
b	[500,250,35]	[0.32,0.5,1.5]	[0.3,0.3,0.4]	0	0	0
c	[200,80,5]	[0.32,0.5,1.5]	[0.3,0.3,0.4]	9000	0.06	0.47
d	[450,200,10]	[0.32,0.5,1.5]	[0.3,0.3,0.4]	[6000,1700]	[0.06,0.25]	[0.5,0.7]
e	[200,75,5]	[0.32,0.5,1.5]	[0.3,0.3,0.4]	9800	0.065	0.43
f	[300,100,25]	[0.32,0.5,1.5]	[0.3,0.3,0.4]	[7500,1000]	[0.06,0.25]	[0.5,0.7]

Table 1. Summary of aerosol initial conditions for experiments in Figure S6. Values in the square brackets represent values for each lognormal mode present. For K-feldspar three lognormal modes were used to represent the aerosol size distribution. In experiments d and f, two lognormal modes were used to represent the ammonium sulphate distribution. In experiments c and e one lognormal mode was sufficient to represent the ammonium sulphate aerosol.

4 Chamber Experiments

A total of six expansion experiments were carried out in MICC. Supplementary Fig. S5 shows example pressure and temperature profiles during an experiment as well as model fits for both. The example shown is typical of all experiments.

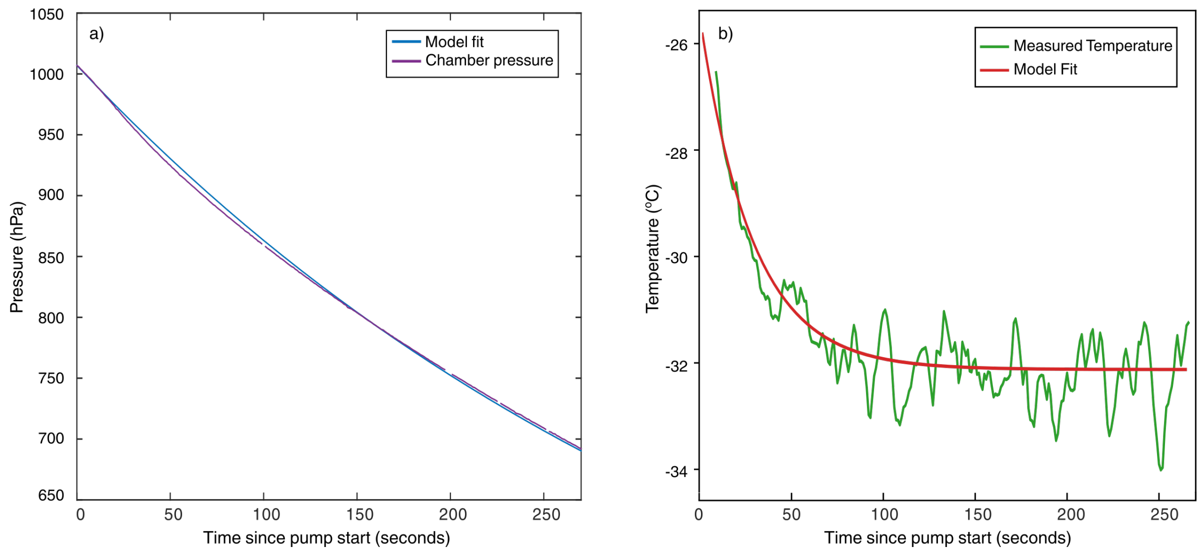

Figure S5. Example fits for pressure and temperature during an expansion experiment. a) The purple line is the pressure measured in the chamber by a Keller pressure sensor. The blue line is the pressure as simulated by ACPIM. b) Green line shows the temperature inside the chamber measured by a thermocouple. The red line is the temperature as simulated by ACPIM.

The thermocouples have a time constant of about 60s, applying this time constant to the measurements insures that at the beginning of an expansion the temperature drop rate in the chamber is quasi-adiabatic until approximately 50 seconds (Supplementary Fig. S5b). See the Appendix of Frey et al. (in review, 2018) for more details.

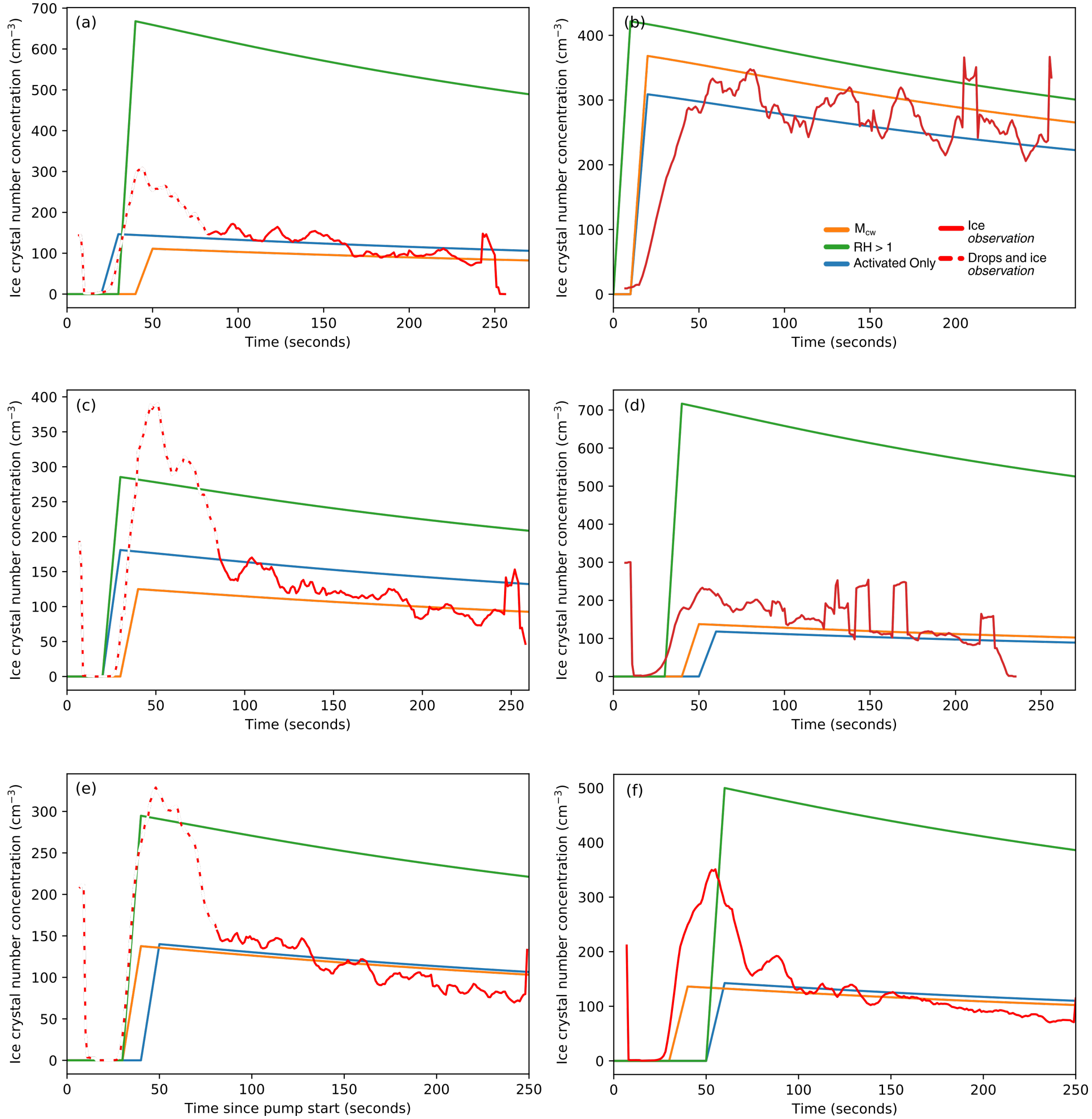

Figure S6. Number concentration of ice crystals in 6 chamber experiments and model simulations using different criteria for freezing. The solid red lines are the number concentration of ice measured in the chamber, dashed red line represents the sum of liquid droplets and ice crystals initially formed and the other coloured lines are simulated ice number concentrations using different criteria for freezing in the model. Aerosol initial conditions given in Supplementary Table 1 for each experiment.

5 Fit used for freezing temperature of solution

Supplementary Figure S7 shows the fit used here for the freezing temperature of a solution when $logJ$ =0 cm^{-3}s^{-1} following the parameterisation for homogeneous freezing by Koop et al. (2000).

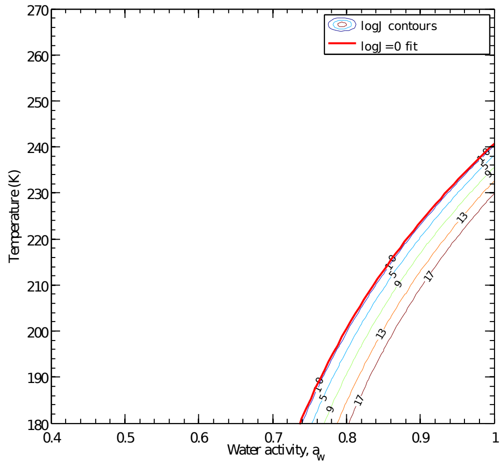

Figure S7. Contours of the homogeneous freezing, J, rate calculated according to the Koop parameterisation, (Koop et al., 2000). Red line is the polynomial fit to the *logJ=0* contour.

6 Additional sensitivities of the suppression effect results

The following figure is similar to Fig. 4. and Fig. 5. however the criteria for freezing is that there must be sufficient water on an INP to overcome the freezing point depression caused by the presence of solutes.

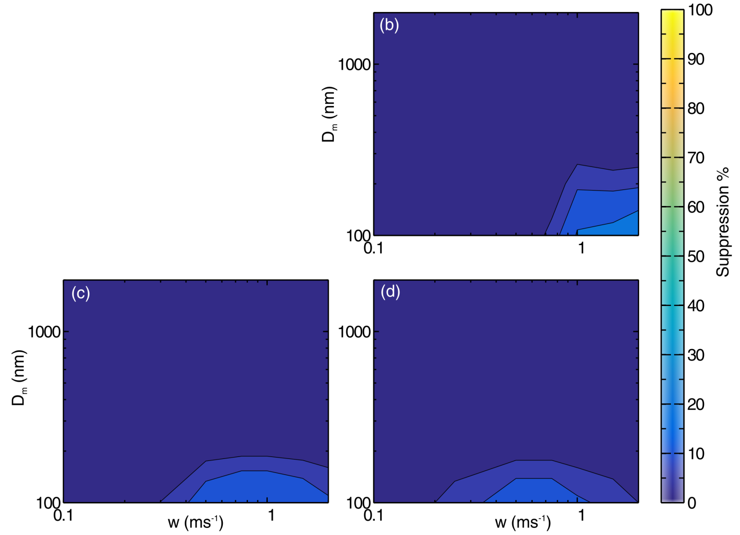

Figure S8. Results from 147 pairs of *low CCN* and *high CCN* model simulations with initial conditions as detailed in tables 3 and 4. the ice crystal number concentration in every simulation was taken at -30^{o}C. Contours show the percentage less ice that formed in the *high CCN* case compared to the *low CCN* case. The criteria for freezing in these results was that there was sufficient water mass on an INP to overcome the freezing point depression caused by the presence of solutes.

The following four figures display results from the same model runs as those shown in Fig. 4. and Fig. 5. however compare ice crystal number concentrations at temperatures warmer than -30^{o}C. The criteria for freezing in Supplementary Fig. S9. and S10. is *Activated only*. The white areas on the top right panel of Supplementary Fig. S9. and the top two panels Supplementary Fig. S10 show negative suppression. This means more ice had formed in the *high CCN* case compared to the *low CCN* case at the point the comparison between the two cases was made. At most this is -2.4 $\%$. At the end of the simulation time, around -30^{o}C shown in Figure 5, there is always higher, or the same, number concentration of ice in the *low CCN* case.

The criteria for freezing in Supplementary Fig. S11. and S12 is M_{cw}.

Additional sensitivity simulations with a representation of desert dust, following Niemand et al. (2012), instead of K-feldspar were preformed. The results from these simulations with two different freezing criteria (*Activated Only* and M_{cw}) are presented in the Supplementary Figs. S13 and S14.

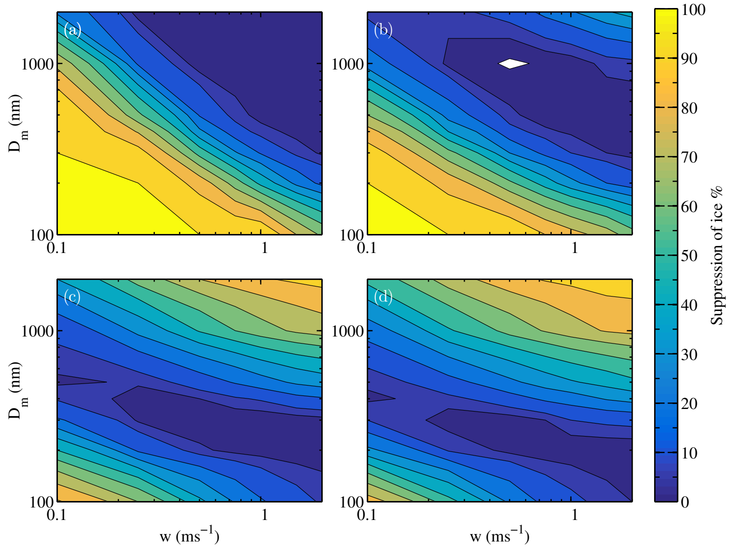

Figure S9. Same model runs as displayed in Figure 4 however with ice concentrations compared at -15^{o}C instead of -30^{o}C.

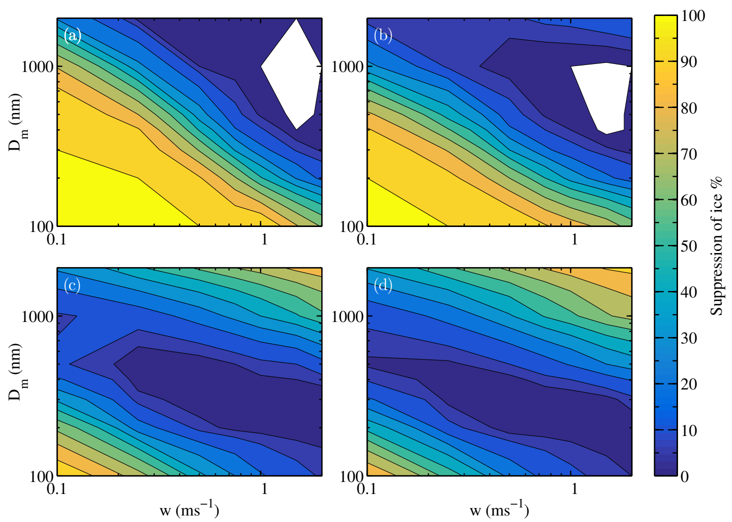

Figure S10. Same model runs as displayed in Figure 5 however with ice concentrations compared at -20^{o}C instead of -30^{o}C.

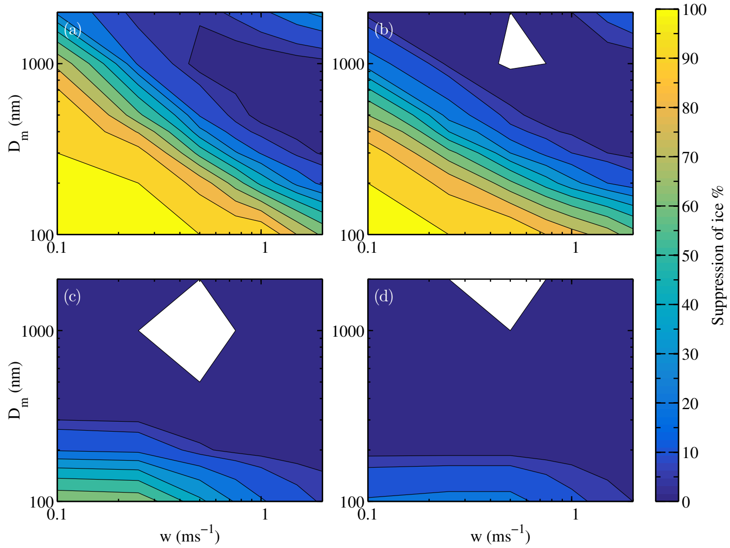

Figure S11. Same model runs as displayed in Figure 5 however with ice concentrations compared at -20^{o}C instead of -30^{o}C.

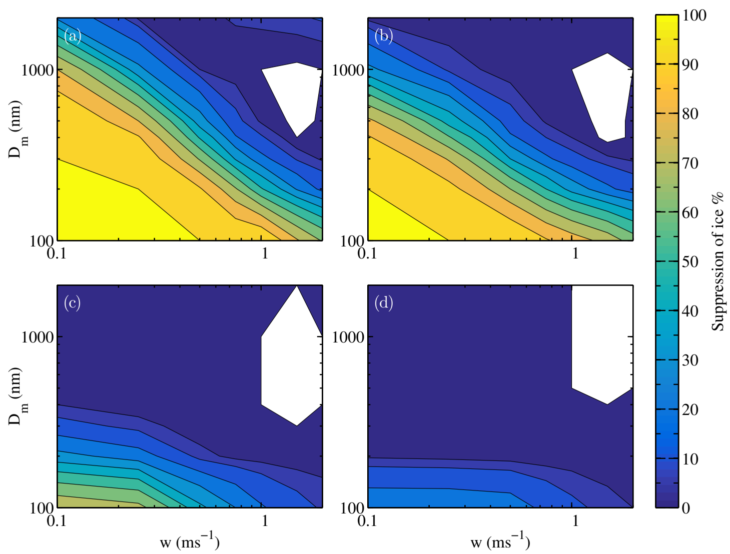

Figure S12. Same model runs as displayed in Figure 5 however with ice concentrations compared at -20^{o}C instead of -30^{o}C.

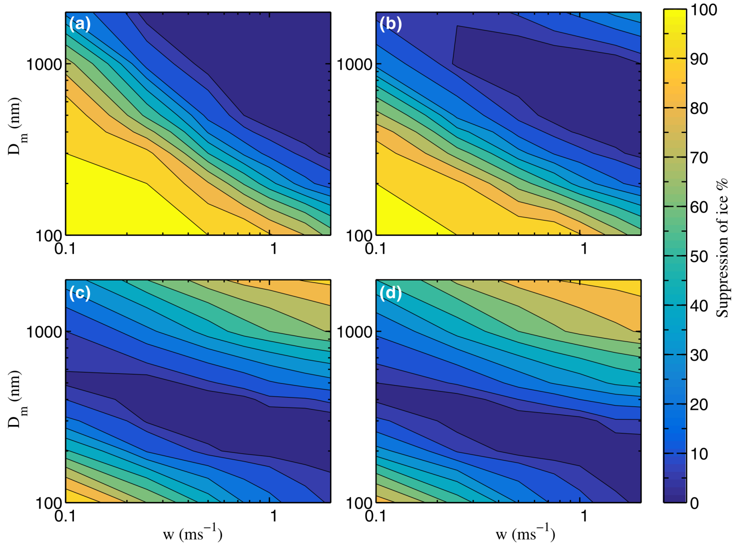

Figure S13. Results from 196 pairs of *low CCN* and *high CCN* model simulations with initial conditions as detailed in Tables 2 and 3 however instead of K-feldspar a representation of desert dust is used for INPs. For each of the four soluble fractions of INP the updraft velocity ranged between 0.1 and 2 ms^{-1} and the diameter of the INP varied between 100 and 2000 nm. The ice crystal number concentration in every simulations was taken at -30^{o}C. Contours show the percentage less ice that formed in the *high CCN* case compared to the *low CCN* case. The criteria for heterogeneous freezing in these results is only activated drops can freeze.

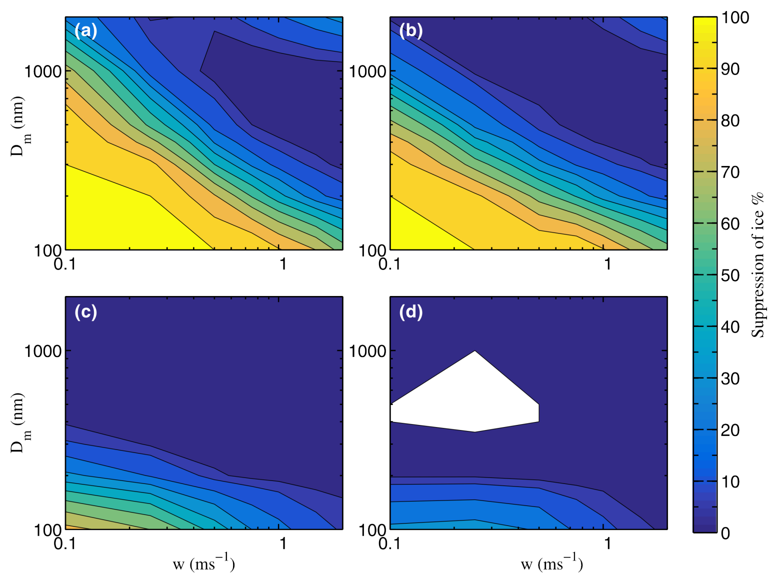

Figure S14. Same as Supplementary Figures S13 however the criteria for freezing is M_{cw}.

7 Comparison of the mass of water required for freezing for two freezing criteria

Under the chamber conditions in this study, T = -25^{o}C, a smaller mass of water is required for a particle with a diameter < 0.8 μm that is 1% soluble to activated than is required to reach M_{cw}. Supplementary Fig. S15a shows the mass of water required by both of the criteria for freezing, M_{cw}, and *Activated Only*, for different particle diameters under chamber conditions. At higher temperatures and for particles with larger soluble fractions the mass of water required to activate a particle is greater than the mass required to reach M_{cw}, this difference is greatest at $D_p > 1$ μm. This is shown in Supplementary Fig. S15b which is similar to Supplementary Fig. S15a, however T = -7^{o}C in the calculation of mass of water required for activation and particles are 25% soluble. Under the conditions in Supplementary Fig. S15b, and for particles with Dp > 0.5 μm, the mass of water required to reach activation is significantly greater than M_{cw}. This means that a particle which does not have enough condensed water to activate and therefore cannot freeze under the criteria of *Activated Only*, could freeze if the criteria for freezing was M_{cw} where a smaller mass of water is required for freezing.

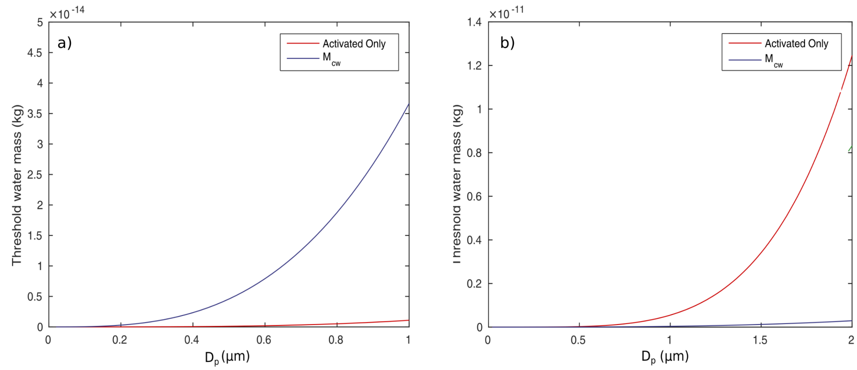

Figure S15. a) A comparison of the threshold mass of water required for freezing for two difference criteria for different particle diameters under chamber conditions, T = -25^{o}C. b) Similar to (a) however for 25% soluble dust particles under similar conditions as found in parcel model simulations, T = -7^o, the results of which are shown in Figs. 4 and 5.

References

Frey, W., Hu, D., Dorsey, J., Alfarra, M. R., Pajunoja, A., Virtanen, A., Connolly, P., and McFiggans, G.: The efficiency of secondary organic aerosol particles to act as ice nucleating particles at mixed-phase cloud conditions, Atmos. Chem. Phys. Discuss., in review, 2018.

Jacobson, M. Z.: “Fundamentals of atmospheric modelling”, “Cambridge University Press”, 1999.

Koop, T., Luo, B., Tsias, A., and Peter, T.: Water activity as the determinant for homogeneous ice nucleation in aqueous solutions, Nature, 406, 611–614, 2000.

Niemand, M., Möhler, O., Vogel, B., Vogel, H., Hoose, C., Connolly, P., Klein, H., Bingemer, H., DeMott, P., Skrotzki, J., and Leisner: A particle-surface-area parameterisation of immersion freezing on desert dust particles, Journal of Atmospheric Sciences, 69, 3077–3092, 2012.